HHS Public Access

Author manuscript

J Pathol. Author manuscript; available in PMC 2016 November 01.

Published in final edited form as:

J Pathol. 2015 June ; 236(2): 142–154. doi:10.1002/path.4506.

Identification of novel vascular projections with cellular trafficking abilities on the microvasculature of pancreatic ductal adenocarcinoma

Saiyin Hexige[#1], **Christine M. Ardito-Abraham**[#2], **Yanhua Wu**[1], **Youheng Wei**[1], **Yuan Fang**[2], **Xu Han**[2], **Jianang Li**[2], **Ping Zhou**[1], **Qing Yi**[3], **Anirban Maitra**[4,5], **Jun O Liu**[6], **David A. Tuveson**[2], **Wenhui Lou**[2], and **Long Yu**[1]

[1] State Key Laboratory of Genetic Engineering, School of Life Sciences, Fudan University, Shanghai, 200433, People's Republic of China

[2] Cold Spring Harbor Laboratory, New York, NY11724, United States of America

[3] General Surgery Department, Zhongshan Hospital, Fudan University, Shanghai, 20032, People's Republic of China

[4]Cleveland Clinic, Lerner Research Institute, Cleveland, Ohio, 44195

[5] Department of Pathology, The University of Texas MD Anderson Cancer Center

[6]Departments of Pharmacology and Oncology, Johns Hopkins School of Medicine, MD 21205, United States of America.

[#] These authors contributed equally to this work.

Abstract

Pancreatic ductal adenocarcinoma (PDAC) is a nearly lethal neoplasm. It is a remarkably stroma-rich, vascular-poor, hypoperfused tumor, which prevents efficient drug delivery. Paradoxically, the neoplastic cells have robust glucose uptake, suggesting the microvasculature has adopted an alternative method for nutrient uptake and cellular trafficking. Using an adapted thick tumor section immunostaining and 3-dimensional (3D) construction imaging method in human tissue samples, we identified an undiscovered feature of the mature and angiostatic microvasculature in advanced PDAC tumors; long, “hairy”-like projections on the basal surface of microvessels that we refer to as “*basal microvilli*”. Functionally, these basal microvilli have an actin-rich cytoskeleton, endocytic and exocytic properties, and they contain glucose transporter-1 (GLUT-1) positive vesicles. Clinically, as was demonstrated by PET-CT, the tumor microvasculature with the longest and the most abundant basal microvilli positively correlated with the high glucose uptake of the PDAC tumor itself. In addition, these basal microvilli were found in regions of the tumor with low GLUT-1 expression, suggesting their presence could be dependent upon the glucose

Correspondence should be addressed to saiyin@fudan.edu.cn, longyu@fudan.edu.cn or wenhuilou@aliyun.cn.

Author contributions: H. S discovered the basal microvilli in PDAC and designed the research project; S.H,Y.Wu, C.M. A-A, Y.F, Y.Wei and P.Z performed experiments ; Y.F, X.H, J.Land W.L collected clinical samples ; S.H, C.M.A-A, A.M and D.T analyzed data; and S.H, C.M.A-A, Q.Y, J.L ,D.T and L.Y wrote the paper.

CONFLICT OF INTEREST

The authors declare no competing financial interests.

concentrations in the tumor milieu. Altogether, these basal microvilli mark a novel, pathological feature of the PDAC tumor microvasculature. Because these basal microvilli are pathological features with endo- and exocytic properties, they may provide a non-conventional method for cellular trafficking in PDAC tumors.

INTRODUCTION

Pancreatic ductal adenocarcinoma (PDAC) is a near uniformly lethal tumor [1]. The extremely poor prognosis for PDAC patients is partially due to resistance to conventional therapeutic modalities [2, 3]. Despite intensive efforts, there are no truly effective therapies available for treating PDAC patients at the moment [4]. One proposed mode of resistance is that elevated interstitial pressures and hypovascularity of PDAC leads to hypoperfusion and decreased delivery of chemotherapy to the PDAC milieu [5, 6]. Interestingly, PDAC tumors still manage to have a high glucose uptake, as assessed by Fluoro-Deoxyglucose positron emission tomography (^{18}FDG-PET) scans [7]. Clinical data has shown that the high glucose uptake/perfusion ratio correlates with a poor outcome for PDAC patients, suggesting that PDAC tumors do not have to be highly perfused to be highly metabolically active [8].

MRI and CT angiography, the standard imaging methods for visualizing vessel perfusion, only visualize blood vessels larger than 100μm in diameter [9]; however, the diameter of microvessels involved in nutrient or drug exchange are far smaller than 100μm [10], which means these type of microvessels have gone undetected. Additionally, pathologists are limited by the use of thin biopsy sections that lack the tissue depth needed to fully observe the multi-dimensional nature of a tumor microvasculature [11]. Altogether, this means that it is impossible to visualize the entire microvasculature by these standard imaging methods. With this, we hypothesized that the PDAC microvasculature remains mostly unexplored and may contain ultrastructural characteristics that have undetected and underappreciated due to these technical limitations. Our aim was to design a better imaging method that would be capable of revealing novel characteristics of microvessels. To reveal the fully functional microvascular network, we immunostained thick tumor tissue sections (45μm-thick) from human PDAC samples, and for the first time by 3D imaging reconstruction, we could visualize in 3D the tumor microvasculature, allowing us to analyze its fine architecture. By means of our modified method, we revealed a novel type of microvessel that contains long, “hairy”-like projections on the basal surface. We named these vascular microstructures “basal microvilli” based on their location and the morphological resemblance to microvillus projections. Basal microvilli have cellular trafficking properties, contain GLUT1 positive vesicles and are prevalent in human PDAC tumors with high glucose uptake, suggesting their possible role in facilitating cellular uptake and trafficking between the tumor cells and the microenvironment. As PDAC tumors are hypoperfused, these basal microvilli may provide a nonconventional, bypass mechanism for nutrient uptake in PDAC microvessels.

Materials and Methods

Materials, methods and patient information are provided in supplementary data.

Ethics

The research was approved by the Clinical Ethical Committee of Zhongshan Hospital, Fudan University.

RESULTS

Human PDAC contains a mature, angiostatic vascular network

To comprehensively characterize the microvessel characteristics in PDAC patients, we immunostained microvessels of thin paraffin sections (5μm) from PDAC patient samples with the endothelial marker, CD34, to image the tumor microvasculature. Then, according to pathological standards, we measured several microvessel parameters: microvessel density [(MVD) the number of microvessels in a given area), size (the area of the microvessel), percent coverage (the percentage of microvessels in a given area/total area) and the perimeter (the distance around the microvessel). We measured the microvessel parameters in PDAC (n=86), a hypovascularized cancer, in hepatocellular carcinoma (HCC, n=39), a neoangiogenic cancer [12], and in the normal pancreas (n=57). The average MVD in PDAC was only 26.5% that of the normal pancreas and 50.0% that of HCC **(Figure 1A)**. The percent of microvessel coverage in PDAC was 40.0% that of the normal pancreas and 28.6% that of HCC **(Figure S1A**). The average size of microvessels in PDAC was 56.7% that of HCC and almost twice that of the normal pancreas **(Figure 1A)**. The average perimeter of microvessels in PDAC was slightly longer (55.2 ±14.22μm) than that observed in the pancreas (41.2 ±7.75μm) and shorter that than observed in HCC (69.1 ±16.94m) **(Figure S1A)**. PDAC tumor vessels appeared to be lacking a branching phenotype, as is commonly seen in angiogenic tumors, like those observed in HCC **(Figure S1B)**. Higher magnification revealed that the morphology of microvessels in PDAC resembled the structure of normal pancreatic microvessels, but differed from the large, dilated microvessels of HCC **(Figure 1B)**. To note, no other significant correlations were observed between the microvessel parameters and prognosis of patients or clinical pathology, including age, gender, location of tumor, tumor stage, regional lymph node status, metastases, TNM and tumor differentiation **(Figure S1C and Table S1)**, as was consistent with a previous report [13]. Angiogenesis in solid tumors initiated by the vascular endothelial growth factor (VEGF), which is released by tumor cells in a hypoxic environment in response to hypoxia-inducible factor (HIF-1α) [14]. Typically, VEGF induced-neoangiogenic microvessels in solid tumors have a dilated lumen [15]; however, PDAC tumors microvessels have been reported to be compressed and hypoperfused [16, 17]. To determine whether the human PDAC tumors have hypoxia-induced, VEGF-mediated angiogenesis, we used tissue microarrays to compare the expression patterns of HIF-1α and VEGFR2 by immunohistochemistry. HIF-1α expression was strong in only 1/12 PDAC samples by immunoblotting **(Figure S2A)**. Immunohistochemistry revealed varying degrees of HIF-1α expression in 88/197 patients **(Figure S2B)**. Additionally, HIF-1α was expressed in neoplastic cells, but mostly in endothelial cells and precancerous lesions in PDAC tumors **(Figure S2B)**. Contrary to a previous report [18], we failed to find any correlation between microvessel parameters, including percentage of microvessel coverage and microvessel size, and HIF-1α expression level in PDAC patients **(Figure S2B)**. Consistent with a previous report [19], we detected significant HIF-1α expression in all HCC (13/13) and liver (3/3) samples (**Figure S2D**).

HIF-1α expression level in HCC patients positively correlated with increased percentage of microvessel coverage and size. HCC tumors with higher levels of HIF-1α had a higher percentage of microvessel coverage and more dilated microvessels **(Figure S2D and S2E)**. In PDAC tumors samples, VEGFR2 was expressed in precancerous lesions and in a limited number of tumor cells, but not in endothelial cells **(Figure S2C)**, whereas VEGFR2 was widely expressed in tumor cells, endothelial cells and infiltrating inflammatory cells in most of the HCC tumors **(Figure S2F)**. Although hypoxia is severe in PDAC [20], spatial and heterogeneous expression patterns of HIF-1α and VEGFR2 imply that the paradigm for hypoxia-induced angiogenesis may not apply universally to PDAC tumors.

Neoangiogenic vessels form from terminal endothelial cells and/or branch points of preexisting vessels, which is accomplished by tip-stalk cell fate specification mediated by VEGF-Notch signaling [21]. A newly-formed, immature sprout is commonly identified by proliferating stalk cells next to terminal end UNC5B-positive tip cell with filapodia [22]. These new sprouts are marked by the presence of nascent pericytes, or even the absence of pericytes and basal membrane [22]. Because of the significantly lower MVD and size of PDAC microvessels, we hypothesized that the human PDAC microvasculature is non-angiogenic, or angiostatic. To assess this possibility, we systematically analyzed immunostained PDAC and HCC tumor sections for the presence of tip cells, proliferating endothelial cells, pericyte coverage and basement membrane integrity. In HCC tumor tissues, we observed two types of endothelial tip cells with filopodia; one at the branch points of preexisting microvessels and the others at the tips of microvessels **(Figure S1D)**. In contrast, there were no terminal endothelial cells with filapodia in the PDAC microvessels (**Figure S1D**). To assess angiogenesis in the tumor microvasculature, we co-immunostained tissues with the endothelial marker, CD34, the proliferation marker, Ki67, and the endothelial tip cell marker, UNC5B. Normally, UNC5B is expressed in the developing vasculature [23] and in tumors where angiogenesis is robust. We observed proliferating endothelial cells at the terminal ends or branch points of HCC microvessels **(Figure 1C)**. However, in PDAC tumors, no proliferating endothelial cells were observed at the terminal ends of the microvessels **(Figure 1C)**. Only a small number of proliferating cells could be observed in the microvessel wall, which is considered to be the result of normal turn-over activity [24]. Quantitatively, the ratio of proliferating endothelial cells to microvessels in HCC was significantly higher than that in PDAC **(Figure 1C)**. In HCC, there was a significantly higher UNC5B-positive endothelial cell to microvessel ratio, compared to PDAC where there were no detectable UNC5B-positive endothelial cells **(Figure 1D)**. Because of the lack of proliferating endothelial cells and of UNC5B-positive tip cells in PDAC, these results infer that PDAC tumors are mostly angiostatic. Next, we evaluated the pericyte coverage of microvessels in PDAC compared to HCC tissue samples. To do this, we co-immunostained tissues with markers for nascent and mature pericytes [NG2 and platelet-derived growth factor receptor (PDGFR)-β, nascent; Desmin and smooth muscle actin (SMA), mature], in combination with endothelial markers (CD31 or CD34). We found that 16.7% of microvessels in HCC were devoid of mature, SMA-positive pericyte coverage, but that all microvessels in PDAC were covered by SMA-positive pericytes **(Figure S3A and Table S2)**. In contrast to the intense staining in stromal cells, most of the microvessel pericytes in PDAC showed weak desmin and PDGFRβ expression **(Figure S3B and S3C)**.

A small number of nascent NG2-positive microvessel pericytes were observed in PDAC, and those pericytes covered the end of smaller microvessels **(Figure S3D)**. In contrast, we counted a significant number of NG2- and PDGFRβ-positive nascent pericytes in HCC microvessels **(Table S2)**. These nascent pericytes were located at the ends of microvessels or were attached to the branching points of microvessels **(Figure S3C and S3D)**. Desmin-positive pericytes in HCC appeared to be loosely attached to the main branches of microvessels **(Figure S3B)**.

Analysis of the PDAC microvasculature demonstrated a quiescent, angiostatic state, therefore, we hypothesized that the PDAC microvessels were of a more mature, co-opted nature than a highly angiogenic vasculature seen in the HCC tumors. To test this, we evaluated the integrity of the microvessel basement membrane as a measurement for vessel maturity in PDAC and HCC by using triple immunofluorescent staining for mature pericytes, endothelial cells and basement membrane type IV collagen. The microvessels in PDAC had a complete basement membrane that was covered with pericyte processes **(Figure S4A)**. However, the microvessels in HCC had an incomplete basement membrane, with some regions of the basal surface not covered by type collagen IV on the basement membrane at all **(Figure S4A**). We examined the endothelial junctions by transmission electron microscopy (TEM) and found that microvessels in PDAC were connected to each other by junctional complexes including tight junctions and intermediate junctions **(Figure S4B)**. Altogether, these results indicate that HCC tumor vessels are immature and angiogenic, while the PDAC vascular network is mature and angiostatic.

Novel “basal microvilli” are vascular projections with an actin cytoskeleton and endo- and exocytic properties on the basal surface of PDAC microvessels

These data indicated that PDAC tumors have a low MVD and a lack of angiogenesis, so we questioned how the tumor cells obtain their nutrients and clear their cellular wastes to support their growth in the absence of an extensive vascular network. While characterizing the PDAC vasculature in tissue samples, we discovered many “hairy”-like, fine vascular projections from the basal surface of most microvessels in human PDAC tumors. These endothelial-derived, basal projections were widely distributed across the microvessels, measuring about 0.8μm to 1.2μm in diameter **(Figure 2A, Movie S1).** In contrast, the basal surfaces of the microvessels in normal human pancreata (n=3) and HCC (n=6) lacked these vascular projections **(Figure 2A, Movie S1)**. The length of basal projections ranged from 3μm to 41μm, and there were about 0.2×10^5-1.3×10^5 microprojections in area unit ($1mm^2$) of a PDAC microvessel. Strikingly, some of the longest projections transversed the perivascular stroma and invaded the neoplastic epithelium **(Figure 2B)**. These endothelial projections do not express another prominent endothelial marker, CD31 **(Figure 2C)**. Additionally, we immunostained for GLUT-1, a glucose transporter highly expressed in red blood cells (RBCs) [25], to determine if the microvascular projections were connected to microvessels with an active blood flow, and in fact, we detected GLUT-1 positive RBCs in the microvessels connected to the endothelial microprojections **(Figure S5A)**.

The functional nature of apical projections in polarized epithelial cells depends on their cytoskeletal properties. Cytoskeletal tubulin is necessary for dynamic movement and the

actin cytoskeleton is necessary for absorptive or secretive functions [26, 27]. We co-immunostained tissues with the cytoskeletal markers, phalloidin (F-action) or α-tubulin and CD34 to further characterize the basal microvilli. Co-immunostaining demonstrated that the cytoskeleton of these projections do not contain tubulin, but contain actin microfilaments that connect to actin filaments of the endothelial cells, similar to how stereocilia and microvilli attach to the cytoplasm of a cell **(Figure 2D and S5B; Figure 2E).**

Endocytosis is the main method by which cells take up and transport macromolecules, and this process can be either clathrin-dependent or clathrin-independent endocytosis [28]. To determine whether basal microvilli have an endocytic capacity, we co-immunostained for CD34 and clathrin, a protein that plays a major role in coating transported vesicles, or ß-COP, a marker for clathrin-independent vesicles, and discovered that basal microvilli contain both types of transporter vesicles **(Figure 3A and 3B).** Transmission electron microscopy (TEM) analysis revealed that these fine microvascular projections contain pinocytic vesicles, phagocytic bodies, macropinocytic pseudopods and large exocytic vesicles, as well as a rough endoplasmic reticulum and mitochondria **(Figure 3C)**. Altogether, these data suggested that these microvascular projections in PDAC tumors may function to increase nutrients transport and waste clearance.

Based on these data, we named these endothelial-derived basal projections as "*basal microvilli*" because of their actin-rich cytoskeleton. Basal microvilli were only observed in malignant, aggressive and metastatic PDAC tumors, but not in non-invasive precursor lesions including pancreatic intraepithelial neoplasia (PanIN)-1, PanIN-2 and PanIN-3 **(Figure S5C-S5F)**. Also, we observed basal microvilli on microvessels in the near-normal pancreas tissue in proximity to the neoplastic regions of GLUT-1 positive tumors **(Figure S5E-S5F; Movie S2)**. These data suggested that basal microvilli are not a physiological, but a pathological phenomenon, that arise only in the setting of invasive PDAC.

Basal microvilli have low levels of phosphorylated VEGFR2

Angiogenesis is induced by tumor production and release of VEGF, the ligand responsible for activating the receptor tyrosine kinase VEGFR2, under hypoxic conditions [14]. VEGF-bound VEGFR2 induces autophosphorylation of specific tyrosine residues [29-31]. Pancreatic neuroendocrine tumor (PanNET) and hemangioblastomas (HB) are very angiogenic tumors, and their neoangiogenic activities are dependent upon activated VEGFR2 signaling [32-34]. However, little is known about the responsiveness of the PDAC vasculature to VEGFR2 signaling. Thus, we were curious if basal microvilli mechanistically resembled VEGF-responsive angiogenic microvessels in other tumor types, so we co-immunostained for VEGFR2 and its active form, phosphorylated VEGFR2^{Y1175} (pVEGFR2^{pY1175}) and VEGFR2^{Y996} (pVEGFR2^{pY996}) with CD34 in PDAC (n=8), PanNET samples (n=3) and HBs (n=6) tumor samples **(Table S3)**. Overall, PDAC microvessels had lower VEGFR2 expression **(Figure S2C)**. In PDAC microvessels, there was a negative correlation; microvessels with high VEGFR2 expression had fewer basal microvilli, while microvessels with low VEGFR2 expression had many basal microvilli **(Figure 4A**). There was a stark contrast in PanNET and HB tumors where there was high VEGFR2 expression distributed along the entire microvessel membrane, including the

filopodia **(Figure 4A, 4B and 4C)**. Additionally, the microvasculature of PanNET and HBs had high pVEGFR2^{Y1175} and pVEGFR2^{Y996} expression, while the basal microvilli extending from the PDAC microvasculature had little to no pVEGFR2 reactivity **(Figure 4C and 4D; Movie S3)**. These data suggest that, unlike microvessel growth seen in the angiogenic tumors, the microvessels and basal microvilli extending from the PDAC microvasculature have low levels of VEGFR2 expression and activation, and thus, may not depend on this signaling pathway for their growth and sustenance.

Basal microvilli may enhance glucose trafficking between the microvessels and neoplastic cells

Based on the robust glucose uptake capacity seen in PDAC patients [7, 35], we hypothesized that the basal microvilli may serve as a conduit for glucose transport to neoplastic cells. ^{18}FDG-PET is a functional imaging method that visualizes the glucose uptake ability of tumors *in vivo*, where the maximal standardized uptake values (SUVmax) are used to semi-quantitatively estimate the glucose uptake ability-radioactivity glucose concentration of the tumor lesions [36]. To determine if there was a correlation of glucose concentration in the tumors relative to the presence of basal microvilli, we compared the characteristics of microvessels with basal microvilli in PDAC patients (n=7) with different SUVmax values. We quantified the length and density of the basal microvilli on microvessels in tumor regions and found that the tumors with high glucose uptake had microvessels containing longer and denser basal microvilli, while tumors with lower glucose concentration had shorter and fewer basal microvilli on the tumor microvessel surface **(Figure 5A, S6A and 5B)**. As the rate of solute exchange of a cell depends on the size of its surface area, we determined that basal microvilli increased the surface area of the microvasculature using an algorithm **(Supplementary Methods)**, and this correlated with high SUVmax values from human patients **(Figure 5B)**. However, human patients' SUVmax values were not dependent upon the percentage of microvessels in the tumor **(Figure S6B).**

Glucose uptake or transport in endothelial cells is facilitated by the glucose transporters (GLUT) family of transmembrane proteins, some via endocytosis and exocytosis [37], and this often depends on the actin cytoskeleton to transport in or through cells [38, 39]. We co-immunostained for CD34, GLUT-1 and phalloidin to determine if actin-containing basal microvilli contain GLUT-1 positive vesicles. Indeed, we detected GLUT-1 positive vesicles within the basal microvilli of microvessels that have active blood flow, and GLUT1 these positive vesicles co-localized with the phalloin-positive actin filaments **(Figure 5C and 5D; Movie S4).** These data indicated that basal microvilli may have the ability to transport glucose into and out of the tumor milieu. While glucose concentration is difficult to directly assess in human tissues, it is well known that GLUT-1 expression levels in cells are sensitive to changes in glucose concentration [40]. To address this possibility *in vitro*, we tested the sensitivity of MiaPaCa-2 cells, to varying glucose concentrations in the medium. We found that GLUT-1 expression depended on glucose concentration in medium, as GLUT-1 expression was low in MiaPaCa-2 cells in high glucose medium, but very high when glucose was absent from the medium **(Figure S6C)**. The change in GLUT-1 expression in MiaPaca-2 cells was fairly rapid, with an increase in GLUT-1 expression only within a few hours post-glucose starvation **(Figure S6C)**. These data suggest that glucose concentrations

have a significant effect on GLUT-1 expression in MiaPaCa-2 cells *in vitro*, thus it is possible that GLUT-1 levels in neoplastic cells reflect the same glucose sensitivity *in vivo.* Although GLUT-1 expression in PDAC neoplastic cells is high, the distribution of GLUT-1 expression in the neoplasia is spatial and appears in a gradient pattern, with some areas very high and some areas very low **(Figure S6D).** Given the uneven GLUT-1 distribution in the tumor, we hypothesized that the presence of basal microvilli was dependent upon GLUT-1 expression in the tumor. To assess the number of basal microvilli in areas with high or low GLUT-1 expression, we co-immunostained PDAC tumors with GLUT-1 and CD34. We found that neoplastic cells with low GLUT-1 expression were in close proximity to microvessels with many, long basal microvilli extending into the neoplastic cells, while those with high levels of GLUT-1 expression were not in close proximity to the microvessels with many long basal microvilli (**Figure 5E, Figure S6E and S6F; Movie S5)**. It implies that the presence of basal microvilli is inversely dependent upon GLUT-1 expression in the neoplasia. In all, these data suggest that these vascular microprojections may play a role in helping the tumor meet its high glucose needs.

KPC mouse tumors recapitulate pathological microvessels in human PDAC

To determine if these basal microvilli could be studied in a genetically engineered mouse model (GEMM) for PDAC, we acquired tumor tissues from the well-established *LSL-Kras$^{G12D/+}$; LSL-Trp53$^{R172H/+}$; Pdx1-Cre* mouse model (referred to as KPC, hereafter), which fully recapitulates the human PDAC pathology [41]. Thick tumor sections from KPC mice were co-immunostained with the aforementioned molecular and cellular markers to measure microvessel characteristics. Excitingly, we discovered that basal microvilli are also present on the basal surface of the tumor vasculature in KPC mice, but not in the near normal regions within the same KPC sample, suggesting these microvessels are pathological in this model **(Figure 6A-6C, Movie S6**). Much like the human PDAC tumors, the basal microvilli were widely distributed and contain actin microfilaments **(Figure 6A and 6B).** The length of the basal microvilli in the KPC tumors was similar to that seen in the human tumors, measuring about 5μm to 41μm long. To determine if the microvessels containing basal microvilli had a blood flow, and if the basal microvilli themselves had a functional lumen, we injected Alexa Fluor 633-labeled lectin into the jugular veins of the KPC mice. As expected due to previous reports [17], we observed little to no fluorescent lectin within the microvessels themselves, making it impossible to determine if the basal microvilli have a functional lumen lumen **(Figure 6C)**. Altogether, these findings suggest that the KPC mouse model recapitulates the human PDAC vasculature, a novel discovery that will allow functional studies of the basal microvilli to be performed.

DISCUSSION

By using this modified immunostaining method, we discovered that PDAC tumors contain pathological vascular microprojections, or basal microvilli. Their actin-rich cytoskeleton and endo- and exocytic properties, along with their expression of GLUT-1 vesicles, suggest that their role is to increase the cell surface area of nutrient exchange of the tumor microvasculature. The presence and abundance of basal microvilli positively correlates to the high glucose uptake of human PDAC tumors. These data reveal an infinitesimal

extension of the PDAC microvasculature that could be supporting the metabolic demands of the growing tumor independent of conventional angiogenesis.

Endothelial cells in normal tissues have apical primary cilium that function as mechanical sensors [42-44] and filopodia that are present only in depolarized endothelial tip cells[45]. Filapodia on tip cells sense guidance cues in the tumor microenvironment and facilitate endothelial cell migration, but do not have active endocytic and exocytic properties [46, 47]. The basal microvilli, however, are not filapodia. Basal microvilli contain both clathrin-dependent and clathrin-independent vesicles, implicating their role in both endo- and exocytosis. Phagocytic and macropinocytic properties are essential for clearing cell debris or macromolecules and tissue fluids to establish and maintain the composition of the tumor microenvironment [48]. Basal microvilli have the pinocytic capabilities much like that seen in a normal microvessels [49], possibly enhancing the phagocytic and macropinocytic activities of PDAC microvessels.

Oncogenic $KRas^{G12D}$, which is present in greater than 90% of PDAC patients, shifts the metabolism of tumor cells from aerobic respiration to anaerobic glycolysis [50, 51]. GLUT-1 is an important membrane transporter of glucose in endothelial cells and in *Ras* mutated neoplastic cells [52, 53]. Basal microvilli contain GLUT-1-positive vesicles and their abundance positively correlates with glucose uptake of human PDAC tumors, suggesting that the basal microvilli are responsible for trafficking glucose into the tumor cells. Furthermore, the spatial decrease in GLUT-1 expression in neoplastic regions of the tumor correlated with longer, denser basal microvilli on the tumor microvessels. Altogether, this suggests that presence of basal microvilli is the microvasculature's response to meet the high metabolic demands of the tumor.

Basal microvilli are pathological and are not present in the microvasculature of normal tissues. This selective expression can be exploited in several therapeutic approaches. First, there is an opportunity to specifically and selectively target the tumor microvasculature while sparing the normal vasculature using selective therapeutics against these vascular microstructures. Or, it is possible to target and ablate the glucose-trafficking basal microvilli as a method of starving the oncogenic $Kras^{G12D}$-dependent tumor cells. High glucose-uptake or high blood glucose in PDAC patients worsens the outcome of patients [54, 55]. Targeting the glucose trafficking abilities of basal microvilli could cut off the lifeline of glucose to the tumor, causing it to regress and possibly improving a patient's outcome. Because the KPC mouse model recapitulates human basal microvilli, these hypotheses can be tested.

Supplementary Material

Refer to Web version on PubMed Central for supplementary material.

ACKNOWLEDGEMENTS

This work was supported in by the Ministry of Education Youth Teacher Fund (KPH1322045), Special Research Fund for Public Welfare Industry of Health and the Translational Research of Early Diagnosis and Comprehensive Treatment in Pancreatic Cancer from Ministry of Health of China (201202007), the National Key Sci-Tech Special Project of China (2008ZX10002-020), the Project of the Shanghai Municipal Science and Technology Commission

(03dz14086), the Changjiang Visiting Scholar Program, and the American Cancer Society (PF-13-317-01). The authors thank Professor Hongbin Lu and Mr. Yulei Ren from Fudan University help with TEM scanning and Ms. Frances Dressman for editorial assistance.

References

1. Jemal A, Siegel R, Ward E, et al. Cancer statistics, 2009. CA Cancer J Clin. 2009; 59:225–249. [PubMed: 19474385]
2. Chu GC, Kimmelman AC, Hezel AF, DePinho RA. Stromal biology of pancreatic cancer. J Cell Biochem. 2007; 101:887–907. [PubMed: 17266048]
3. Neesse A, Michl P, Frese KK, et al. Stromal biology and therapy in pancreatic cancer. Gut. 2011; 60:861–868. [PubMed: 20966025]
4. Stathis A, Moore MJ. Advanced pancreatic carcinoma: current treatment and future challenges. Nat Rev Clin Oncol. 2010; 7:163–172. [PubMed: 20101258]
5. Feig C, Gopinathan A, Neesse A, et al. The pancreas cancer microenvironment. Clin Cancer Res. 2012; 18:4266–4276. [PubMed: 22896693]
6. Provenzano PP, Hingorani SR. Hyaluronan, fluid pressure, and stromal resistance in pancreas cancer. Br J Cancer. 2013; 108:1–8. [PubMed: 23299539]
7. Serrano OK, Chaudhry MA, Leach SD. The role of PET scanning in pancreatic cancer. Adv Surg. 2010; 44:313–325. [PubMed: 20919529]
8. Karreth FA, Tuveson DA. Modelling oncogenic Ras/Raf signalling in the mouse. Curr Opin Genet Dev. 2009; 19:4–11. [PubMed: 19201597]
9. McDonald DM, Choyke PL. Imaging of angiogenesis: from microscope to clinic. Nat Med. 2003; 9:713–725. [PubMed: 12778170]
10. Yuan SY, Rigor RR. In Regulation of Endothelial Barrier Function. San Rafael (CA). 2010
11. Hlatky L, Hahnfeldt P, Folkman J. Clinical application of antiangiogenic therapy: microvessel density, what it does and doesn't tell us. J Natl Cancer Inst. 2002; 94:883–893. [PubMed: 12072542]
12. Semela D, Dufour JF. Angiogenesis and hepatocellular carcinoma. J Hepatol. 2004; 41:864–880. [PubMed: 15519663]
13. van der Zee JA, van Eijck CH, Hop WC, et al. Angiogenesis: a prognostic determinant in pancreatic cancer? Eur J Cancer. 2011; 47:2576–2584. [PubMed: 21958461]
14. Carmeliet P, Jain RK. Angiogenesis in cancer and other diseases. Nature. 2000; 407:249–257. [PubMed: 11001068]
15. Jain RK, di Tomaso E, Duda DG, et al. Angiogenesis in brain tumours. Nat Rev Neurosci. 2007; 8:610–622. [PubMed: 17643088]
16. Olive KP, Jacobetz MA, Davidson CJ, et al. Inhibition of Hedgehog signaling enhances delivery of chemotherapy in a mouse model of pancreatic cancer. Science. 2009; 324:1457–1461. [PubMed: 19460966]
17. Jacobetz MA, Chan DS, Neesse A, et al. Hyaluronan impairs vascular function and drug delivery in a mouse model of pancreatic cancer. Gut. 2013; 62:112–120. [PubMed: 22466618]
18. Sun HC, Qiu ZJ, Liu J, et al. Expression of hypoxia-inducible factor-1 alpha and associated proteins in pancreatic ductal adenocarcinoma and their impact on prognosis. Int J Oncol. 2007; 30:1359–1367. [PubMed: 17487356]
19. Dai CX, Gao Q, Qiu SJ, et al. Hypoxia-inducible factor-1 alpha, in association with inflammation, angiogenesis and MYC, is a critical prognostic factor in patients with HCC after surgery. BMC Cancer. 2009; 9:418. [PubMed: 19948069]
20. Koong AC, Mehta VK, Le QT, et al. Pancreatic tumors show high levels of hypoxia. Int J Radiat Oncol Biol Phys. 2000; 48:919–922. [PubMed: 11072146]
21. Phng LK, Gerhardt H. Angiogenesis: a team effort coordinated by notch. Dev Cell. 2009; 16:196–208. [PubMed: 19217422]
22. Potente M, Gerhardt H, Carmeliet P. Basic and therapeutic aspects of angiogenesis. Cell. 2011; 146:873–887. [PubMed: 21925313]

23. Lu X, Le Noble F, Yuan L, et al. The netrin receptor UNC5B mediates guidance events controlling morphogenesis of the vascular system. Nature. 2004; 432:179–186. [PubMed: 15510105]
24. Vracko R, Benditt EP. Capillary lamina thickening. Its relationship to endothelial cell death and replacement. J Cell Biol. 1970; 47:281–285. [PubMed: 5513555]
25. Montel-Hagen A, Blanc L, Boyer-Clavel M, et al. The Glut1 and Glut4 glucose transporters are differentially expressed during perinatal and postnatal erythropoiesis. Blood. 2008; 112:4729–4738. [PubMed: 18796630]
26. Satir P, Christensen ST. Overview of structure and function of mammalian cilia. Annu Rev Physiol. 2007; 69:377–400. [PubMed: 17009929]
27. Lange K. Fundamental role of microvilli in the main functions of differentiated cells: Outline of an universal regulating and signaling system at the cell periphery. J Cell Physiol. 2011; 226:896–927. [PubMed: 20607764]
28. Grant BD, Donaldson JG. Pathways and mechanisms of endocytic recycling. Nat Rev Mol Cell Biol. 2009; 10:597–608. [PubMed: 19696797]
29. Sinha S, Vohra PK, Bhattacharya R, et al. Dopamine regulates phosphorylation of VEGF receptor 2 by engaging Src-homology-2-domain-containing protein tyrosine phosphatase 2. J Cell Sci. 2009; 122:3385–3392. [PubMed: 19706677]
30. Cross MJ, Claesson-Welsh L. FGF and VEGF function in angiogenesis: signalling pathways, biological responses and therapeutic inhibition. Trends Pharmacol Sci. 2001; 22:201–207. [PubMed: 11282421]
31. Wedam SB, Low JA, Yang SX, et al. Antiangiogenic and antitumor effects of bevacizumab in patients with inflammatory and locally advanced breast cancer. Journal of Clinical Oncology. 2006; 24:769–777. [PubMed: 16391297]
32. Couvelard A, O'Toole D, Turley H, et al. Microvascular density and hypoxia-inducible factor pathway in pancreatic endocrine tumours: negative correlation of microvascular density and VEGF expression with tumour progression. Br J Cancer. 2005; 92:94–101. [PubMed: 15558070]
33. Raymond E, Dahan L, Raoul JL, et al. Sunitinib malate for the treatment of pancreatic neuroendocrine tumors. N Engl J Med. 2011; 364:501–513. [PubMed: 21306237]
34. Hatva E, Bohling T, Jaaskelainen J, et al. Vascular growth factors and receptors in capillary hemangioblastomas and hemangiopericytomas. Am J Pathol. 1996; 148:763–775. [PubMed: 8774132]
35. Higashi T, Saga T, Nakamoto Y, et al. Relationship between retention index in dual-phase (18)F-FDG PET, and hexokinase-II and glucose transporter-1 expression in pancreatic cancer. J Nucl Med. 2002; 43:173–180. [PubMed: 11850481]
36. Friess H, Langhans J, Ebert M, et al. Diagnosis of pancreatic cancer by 2[18F]-fluoro-2-deoxy-D-glucose positron emission tomography. Gut. 1995; 36:771–777. [PubMed: 7797130]
37. Mueckler M. Facilitative glucose transporters. Eur J Biochem. 1994; 219:713–725. [PubMed: 8112322]
38. Klip A, Sun Y, Chiu TT, Foley KP. Signal transduction meets vesicle traffic: the software and hardware of GLUT4 translocation. American Journal of Physiology-Cell Physiology. 2014; 306:C879–C886. [PubMed: 24598362]
39. Tsakiridis T, Vranic M, Klip A. Disassembly of the actin network inhibits insulin-dependent stimulation of glucose transport and prevents recruitment of glucose transporters to the plasma membrane. J Biol Chem. 1994; 269:29934–29942. [PubMed: 7961991]
40. Ogura K, Sakata M, Yamaguchi M, et al. High concentration of glucose decreases glucose transporter-1 expression in mouse placenta in vitro and in vivo. J Endocrinol. 1999; 160:443–452. [PubMed: 10076190]
41. Hingorani SR, Wang L, Multani AS, et al. Trp53R172H and KrasG12D cooperate to promote chromosomal instability and widely metastatic pancreatic ductal adenocarcinoma in mice. Cancer Cell. 2005; 7:469–483. [PubMed: 15894267]
42. Egorova AD, van der Heiden K, Poelmann RE, Hierck BP. Primary cilia as biomechanical sensors in regulating endothelial function. Differentiation. 2012; 83:S56–61. [PubMed: 22169885]
43. Goetz JG, Steed E, Ferreira RR, et al. Endothelial cilia mediate low flow sensing during zebrafish vascular development. Cell Rep. 2014; 6:799–808. [PubMed: 24561257]

44. Jones TJ, Adapala RK, Geldenhuys WJ, et al. Primary Cilia Regulates the Directional Migration and Barrier Integrity of Endothelial Cells Through the Modulation of Hsp27 Dependent Actin Cytoskeletal Organization. Journal of Cellular Physiology. 2012; 227:70–76. [PubMed: 21837772]
45. Carmeliet P, Jain RK. Molecular mechanisms and clinical applications of angiogenesis. Nature. 2011; 473:298–307. [PubMed: 21593862]
46. Virgintino D, Rizzi M, Errede M, et al. Plasma membrane-derived microvesicles released from tip endothelial cells during vascular sprouting. Angiogenesis. 2012; 15:761–769. [PubMed: 22886085]
47. Niles WD, Malik AB. Endocytosis and exocytosis events regulate vesicle traffic in endothelial cells. J Membr Biol. 1999; 167:85–101. [PubMed: 9878078]
48. Swanson JA. Shaping cups into phagosomes and macropinosomes. Nat Rev Mol Cell Biol. 2008; 9:639–649. [PubMed: 18612320]
49. Marchesi VT. The role of pinocytic vesicles in the transport of materials across the walls of small blood vessels. Invest Ophthalmol. 1965; 4:1111–1121. [PubMed: 5321528]
50. Biankin AV, Waddell N, Kassahn KS, et al. Pancreatic cancer genomes reveal aberrations in axon guidance pathway genes. Nature. 2012; 491:399–405. [PubMed: 23103869]
51. Ying H, Kimmelman AC, Lyssiotis CA, et al. Oncogenic Kras maintains pancreatic tumors through regulation of anabolic glucose metabolism. Cell. 2012; 149:656–670. [PubMed: 22541435]
52. Mann GE, Yudilevich DL, Sobrevia L. Regulation of amino acid and glucose transporters in endothelial and smooth muscle cells. Physiol Rev. 2003; 83:183–252. [PubMed: 12506130]
53. Calvo MB, Figueroa A, Pulido EG, et al. Potential role of sugar transporters in cancer and their relationship with anticancer therapy. Int J Endocrinol. 20102010
54. Schellenberg D, Quon A, Minn AY, et al. 18Fluorodeoxyglucose PET is prognostic of progression-free and overall survival in locally advanced pancreas cancer treated with stereotactic radiotherapy. Int J Radiat Oncol Biol Phys. 2010; 77:1420–1425. [PubMed: 20056345]
55. Gapstur SM, Gann PH, Lowe W, et al. Abnormal glucose metabolism and pancreatic cancer mortality. JAMA. 2000; 283:2552–2558. [PubMed: 10815119]

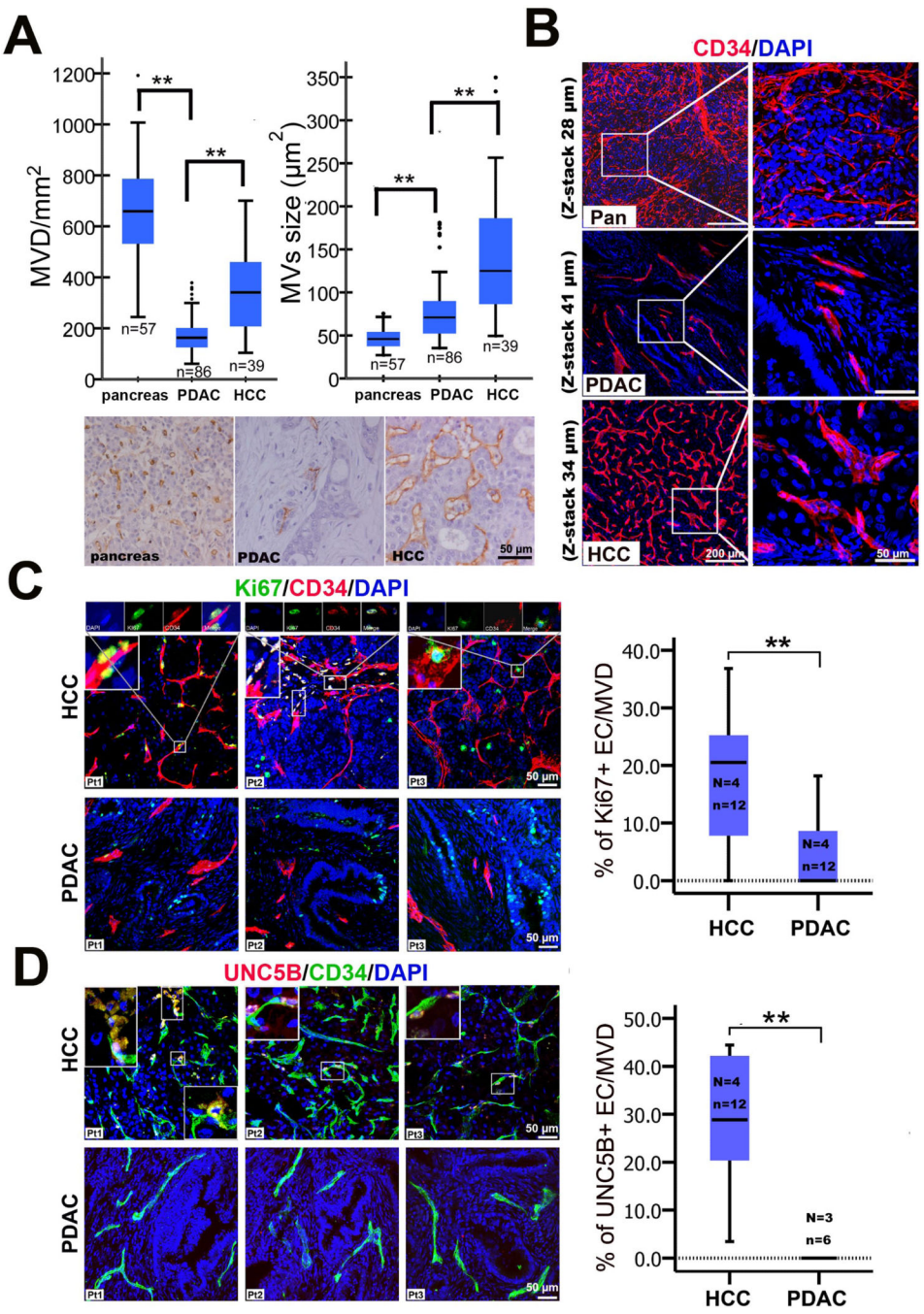

Figure 1. Human PDAC contains an angiostatic vascular network

(A) Comparison of standard microvessel parameters of PDAC with those of pancreas and of HCC. ** $P < 0.01$, using one-way anova. **(B)** 3D images of CD34 immunostained microvessel network in human PDAC, pancreas and HCC tissues. **(C)** Comparison of proliferating endothelial cells in PDAC with that in HCC. Boxed panels show Ki67-positive endothelial cells in HCC located at the tip of a microvessel [Patient 1 (Pt1)], having migrated from the tips of microvessels (Pt2), or at the branch points of microvessels (Pt3). **(D)** Comparison of UNC5B-positive endothelial cells in PDAC with those in HCC. Boxed

panels show UNC5B-positive endothelial cells migrating from the top of microvessels (Pt1, upper left) and UNC5B-positive endothelial cells at the branch points of microvessels (Pt1 & Pt2, lower right) or located at the tip of microvessels in HCC (Pt2 & Pt3). Total UNC5B positive endothelial cells/microvessels count in HCC (138/500) and PDAC (0/77): UNC5B positive cells/total microvessels count; EC, endothelial cells. Statistical significance was assessed by student *t* test. (N = number of patients; n = number of images examined). Values are mean ± SD.

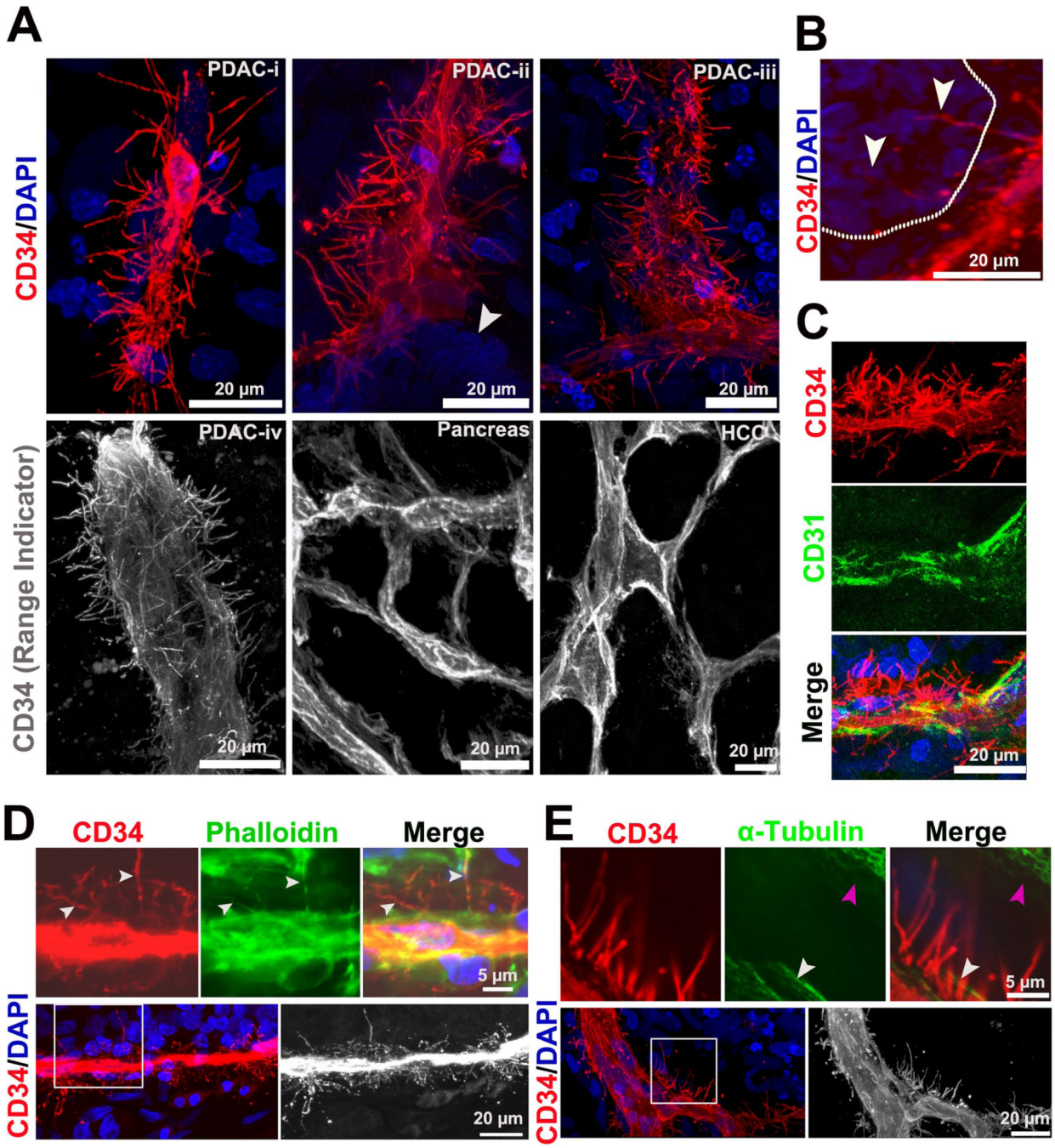

Figure 2. Basal microvilli are actin-rich vascular microprojections on the basal surface of PDAC microvessels

(A) CD34 immunostained 3D images of the basal surface appearance of PDAC, normal pancreas and HCC microvessels (PDAC microvessels diameters: i, 5μm; ii, 10 μm; iii, 20μm and iv, 35 μm; white arrow, neoplastic cells). See **Movie S1**. **(B)** Long basal endocila invade into PDAC neoplastic cells (white dotted line represents the separation of neoplastic cell layer and stroma; white arrows, basal microvilli). **(C)** Co-immunostaining of basal microvilli with CD34 and CD31. **(D)** Co-immunostaining for Phalloidin and CD34 labels the actin

cytoskeleton of basal microvilli in PDAC tissue (white arrow, actin cytoskeleton and basal microvilli). **(E)** Co-immunostaining for α-tubulin and CD34 shows no α-tubulin in basal microvilli of PDAC endothelial cells (white arrow, endothelial cell; pink arrow, stroma cell).

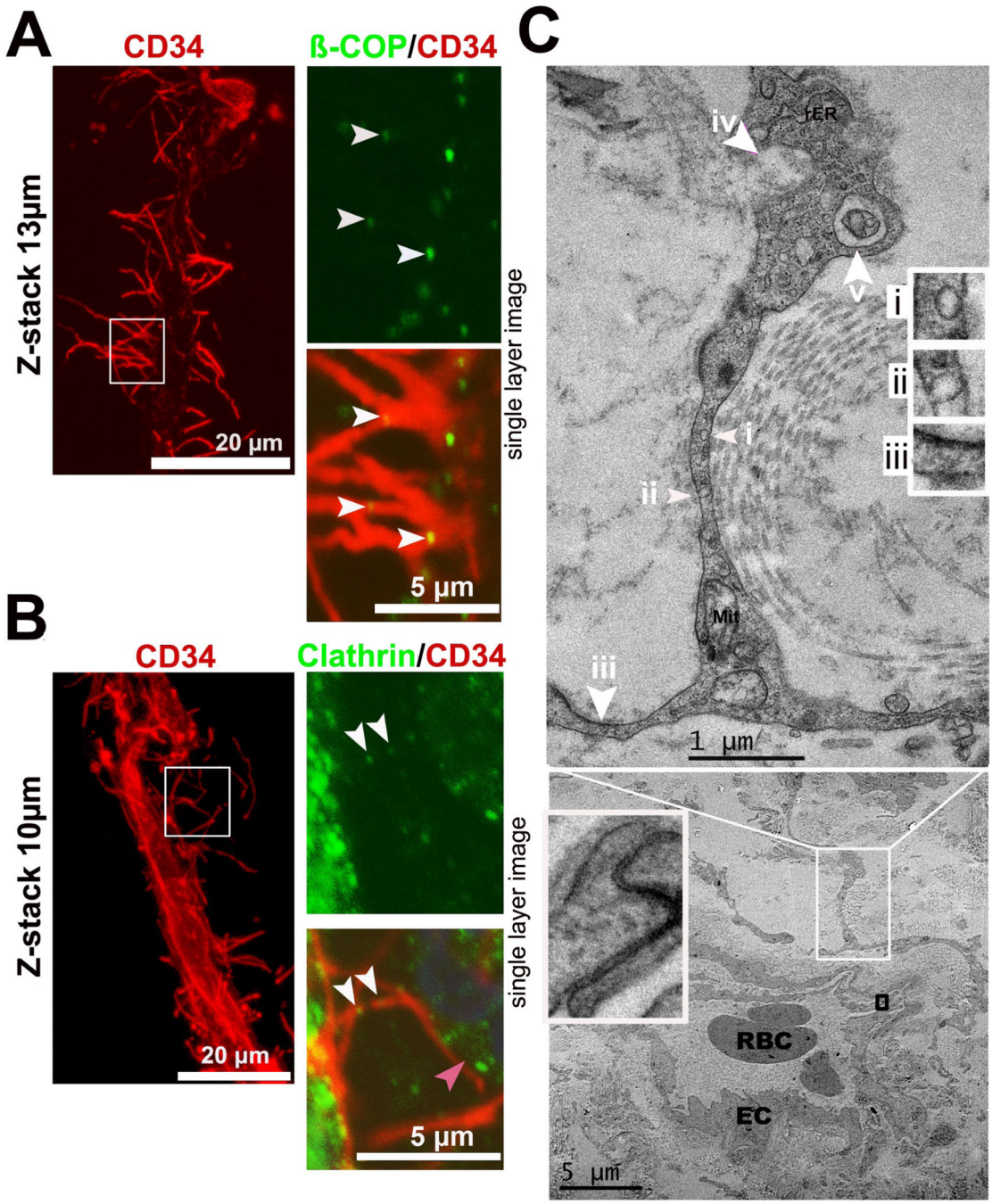

Figure 3. Basal microvilli have cellular uptake and trafficking capabilities

(A), (B) Co-immunostaining for ß-COP or clathrin with endothelial CD34 shows vesicular trafficking in basal microvilli in PDAC (white arrows, ß-COP or clathrin-positive vesicles in microvilli; right panel, a single plane image). **(C)** Ultrastructural features of the basal microvilli of a microvessel in PDAC by TEM (i and ii, pinocytic vesicle; iii, macropinocytic pseudopod with electron dense particles on one side; iv, exocytosis; v, phagocytic vesicles; EC, endothelial cell; Mit, mitochondria; rER, rough endoplasm reticulum).

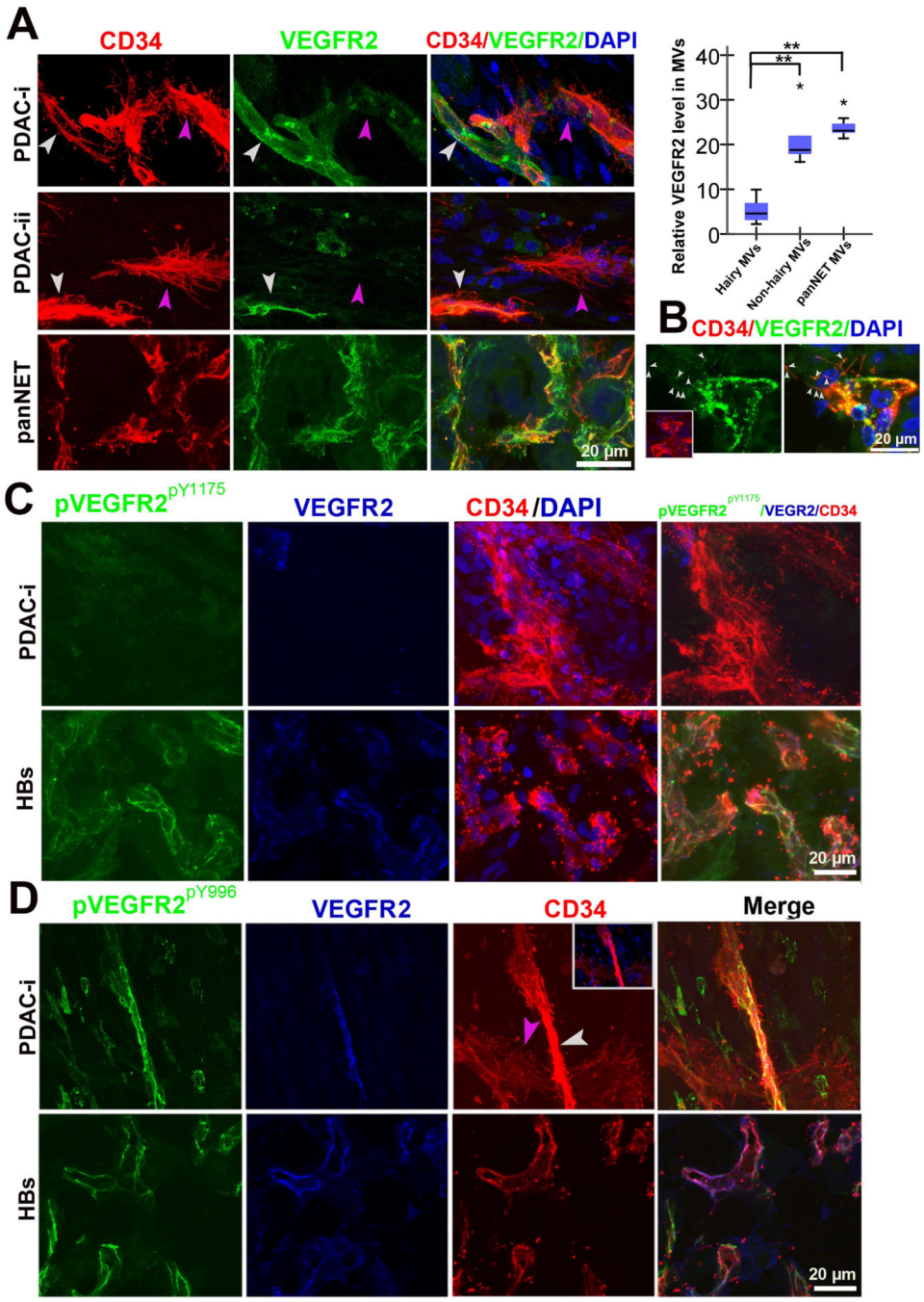

Figure 4. Low VEGFR2 expression and phosphorylation in microvessels that possess basal microvilli

(A) VEGFR2 expression patterns in PDAC “hairy” or “non-hairy”microvessels and PanNET microvessels and endothelial tip cells (PDAC: yellow arrows, “non-hairy” microvessel; pink arrow, hairy microvessels; PanNET: small white arrows, VEGFR2 positive dots on filopodia). Quantitative analysis comparing VEGFR2 levels in “hairy” microvessels with “non-hairy”microvessels of PDAC and microvessels of PanNET. Statistical significance was assessed by student *t* test. **(B)** VERGR2 expression patterns in terminal endothelial cells of the PanNET microvasculature (white arrows, the VEGFR2 positive dots on filopodia). **(C)**

Phospho-VEGFR2^{Y1175} (pVEGFR2^{Y1175}) levels in “hairy” microvessels of PDAC and microvasculature in HBs. **(D)** Phospho-VEGFR2^{Y996} (pVEGFR2^{Y996}) levels in “hairy”or “non-hairy” microvessels of PDAC and microvasculature in HBs (white arrow, “non-hairy” microvessels; pink arrow, “hairy” microvessels). See **Movie S3**.

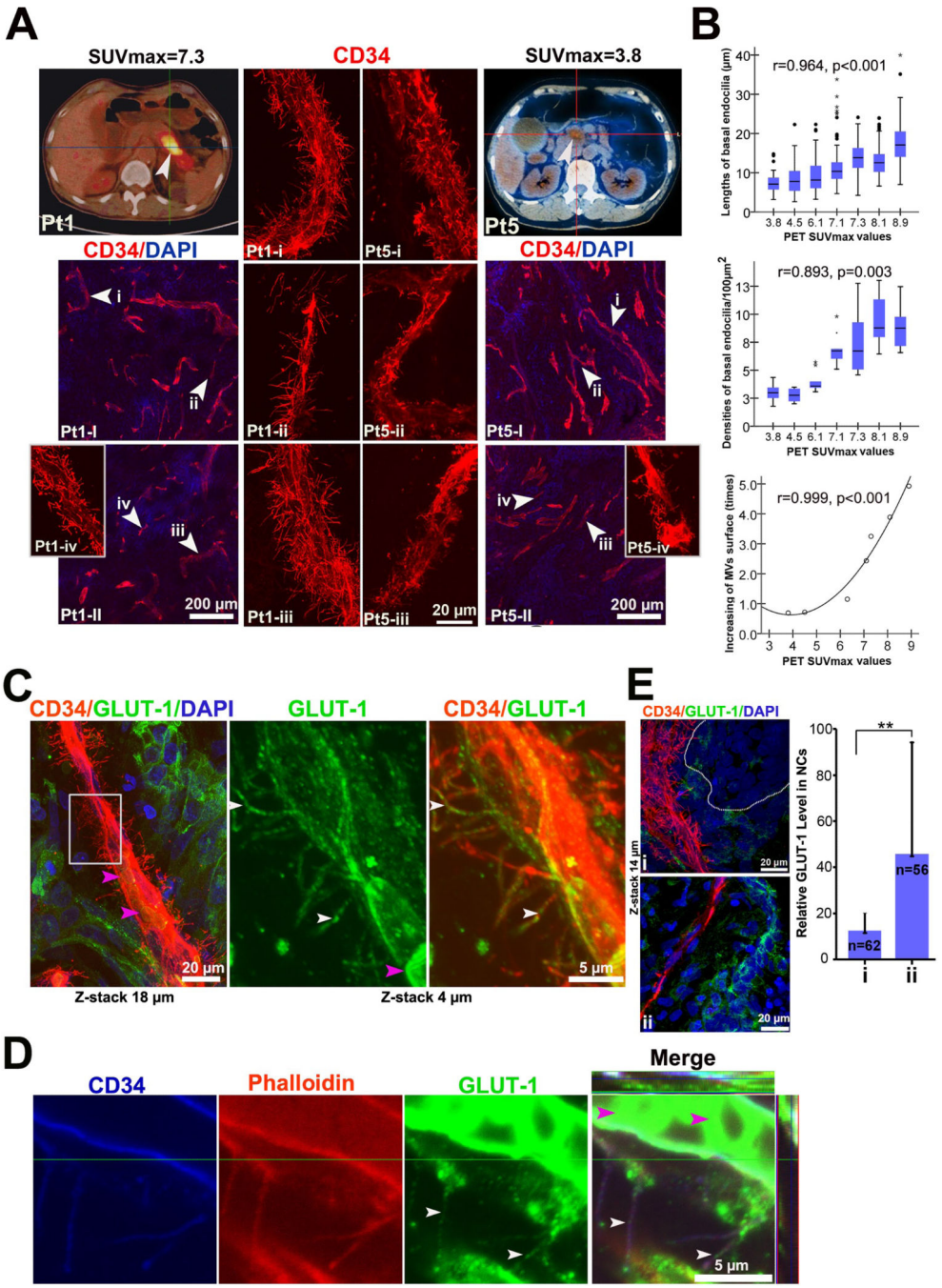

Figure 5. High glucose uptake in PDAC tumors with extensive basal microvilli

(A) Representative images of glucose uptake using ^{18}FDG-PET imaging and characteristics of basal microvilli in PDAC patients. ^{18}FDG-PET images and 3D microvessel images of two PDAC patients (Pt1, a 68 year old man with SUVmax=7.3, tumor size=5.20×2.60cm; Pt5, a 74 year old man with SUVmax= 3.8, tumor size=2.52×1.92cm). Trans-axial PET images reveal high focal ^{18}FDG accumulation in the region of the pancreatic body (Pt1) and moderate in head (Pt5) (white arrows, tumor mass; scanning 60-minutes after injection of ^{18}FDG). **(B)** The relationship between SUVmax values of patients with the lengths and

density of microvessel basal microvilli of seven patient tumors. Statistical significances were performed by Spearsman correlation. **(C)** GLUT-1 positive basal microvilli on the PDAC microvasculature with RBC in microvessel lumen (white arrows, GLUT-1 positive vesicles; pink arrow, RBC). See **Movie S4**. **(D)** Co-immunostaining for Phalloidin, CD34 and GLUT-1 showed that GLUT-1 vesicles co-localized with actin cytoskeleton of basal microvilli on PDAC microvessels (white arrow, GLUT-1 vesicles; pink arrow, RBC). See **Movie S4**. **(E)** GLUT-1 expression in areas of PDAC tumor with a high and low density of basal microvilli (circled regions, neoplastic ducts; n, neoplastic cell count).

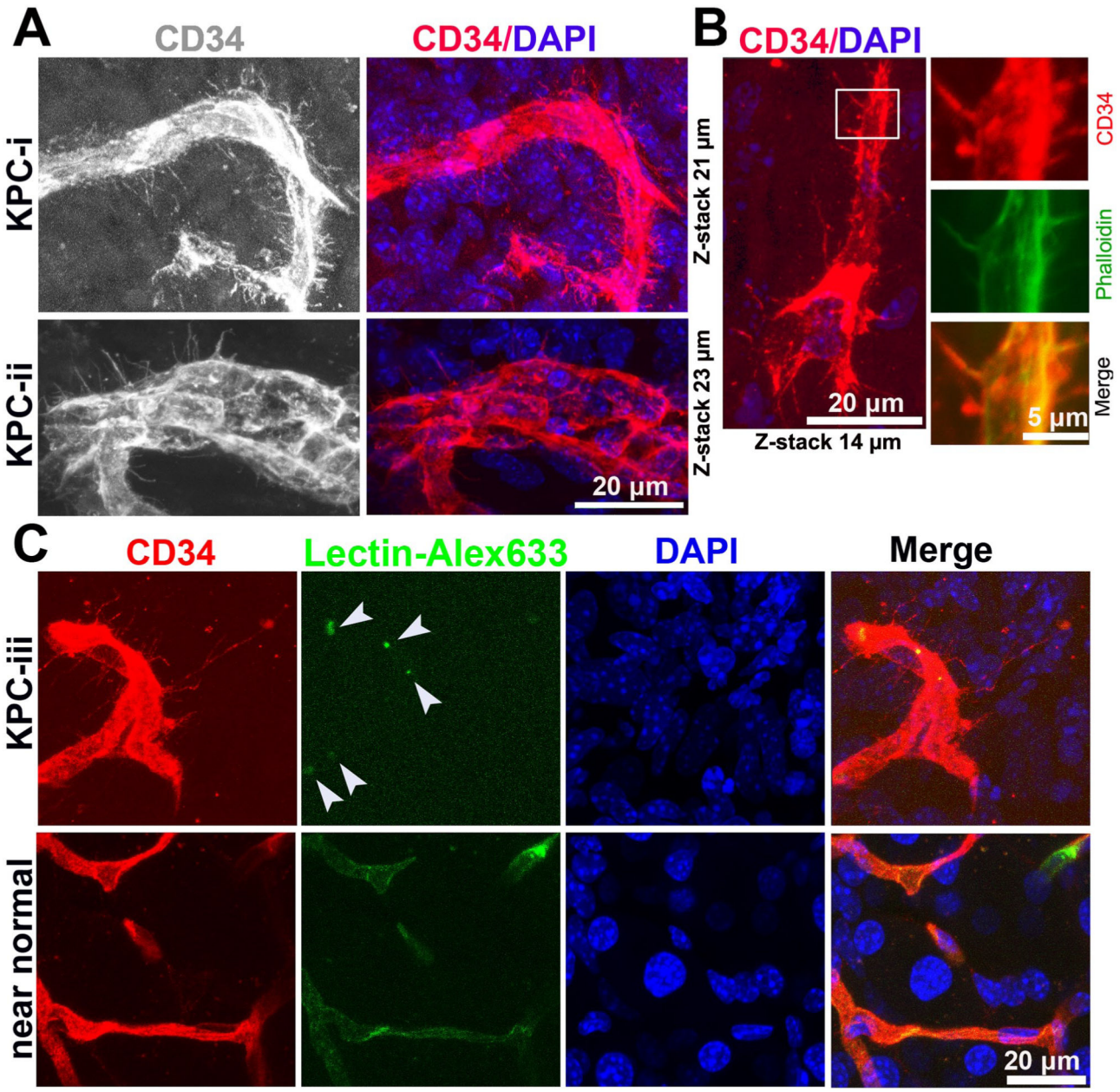

Figure 6. KPC mouse tumors recapitulate pathological microvessels of human PDAC

(A) 3D images of CD34 stained microvessels in KPC mice tumors (microvessels diameter, 10μm; microvessel diameter, 20μm). See **Movie S6**. **(B)** Phalloidin and CD34 co-immunostaining reveals the actin cytoskeleton of basal microvilli in KPC tumor tissue (microvessels diameter, 5 μm). **(C)** 3D images of CD34 stained microvessels in KPC mice tumors and near normal KPC mice tissue perfused by Alexa Fluor 633 conjugated lectin (white arrow, lectin). See **Movie S6**.